

Article

Fabrication of Superhydrophobic Coatings by Using Spraying and Analysis of Their Anti-Icing Properties

Lei Fan ^{1,2}, Mingyong Xia ³, Jian Liu ³, Bo Li ¹, Tao Zhu ², Yingying Zhao ², Linbo Song ² and Yuan Yuan ^{2,*} 

¹ Electric Power Research Institute of Guizhou Power Grid Co., Ltd., Guiyang 550002, China; 15121629726@163.com (L.F.); gzyylb2207@163.com (B.L.)

² College of Materials Science and Engineering, Chongqing University, Chongqing 400044, China; davezhu@cqu.edu.cn (T.Z.); 20193002@cqu.edu.cn (Y.Z.); 202109021149t@cqu.edu.cn (L.S.)

³ Guizhou Chuangxing Electric Power Research Institute Co., Ltd., Guiyang 550081, China; xiamingyong0817@163.com (M.X.); liujian.2@163.com (J.L.)

* Correspondence: yuany@cqu.edu.cn

Abstract: Ice accumulation on glass insulators is likely to cause faults such as flashover, tripping and power failure, which interfere with the normal operation of the power grid. Accordingly, superhydrophobic coatings with great anti-icing potential have received much attention. In this study, three superhydrophobic coatings (PTFE, Al₂O₃ and SiO₂) were successfully prepared on glass surfaces by using one-step spraying. The microscopic morphology, wettability, anti-icing and anti-glaze icing properties of the superhydrophobic coatings were comparatively analyzed. The results indicated that the PTFE coating had a densely distributed rough structure, showing a contact angle of 165.5° and a sliding angle of 3.1°. The water droplets on the surface could rebound five times. Compared with the Al₂O₃ and SiO₂ coatings, the anti-icing performance of the PTFE coating was significantly improved. The freezing time was far more than 16 times that of glass (4898.7 s), and the ice adhesion strength was 9 times lower than that of glass (27.5 kPa). The glaze icing test in the artificial climate chamber showed that the icing weight of the PTFE coating was 1.38 g, which was about 32% lower than that of the glass. In addition, the icing/melting and abrasion cycles destroyed the low-surface-energy substances and nanostructures on the surface, leading to the degradation of the anti-icing durability of the PTFE coatings. However, the PTFE coating still maintained excellent hydrophobicity and anti-icing properties after UV irradiation for up to 624 h. The superhydrophobic coatings prepared in this work have promising development prospects and offer experimental guidance for the application of anti-icing coatings on glass insulators.

Keywords: superhydrophobic coating; glass insulator; spraying; anti-icing



Citation: Fan, L.; Xia, M.; Liu, J.; Li, B.; Zhu, T.; Zhao, Y.; Song, L.; Yuan, Y. Fabrication of Superhydrophobic Coatings by Using Spraying and Analysis of Their Anti-Icing Properties. *Coatings* **2023**, *13*, 1792. <https://doi.org/10.3390/coatings13101792>

Academic Editor: Alexandra Muñoz-Bonilla

Received: 12 September 2023
Revised: 7 October 2023
Accepted: 12 October 2023
Published: 19 October 2023



Copyright: © 2023 by the authors. Licensee MDPI, Basel, Switzerland. This article is an open access article distributed under the terms and conditions of the Creative Commons Attribution (CC BY) license (<https://creativecommons.org/licenses/by/4.0/>).

1. Introduction

Icing is one of the common natural disasters on transmission lines, which not only interferes with the normal operation of society and industry but also seriously threatens the stable operation of power systems [1–3]. As an important component of the transmission lines, the icing on the surface of glass insulators can trigger flashover or even loss of electrical insulation, which, in turn, causes the line single-phase ground short-circuit fault trip [4–6]. Traditional hydrophobic coatings (RTV and PRTV) applied on glass insulators have a good anti-fouling effect but cannot solve the problem of surface ice-covering [7–9]. Mechanical deicing and current ice melting are more widely used in engineering practice. However, the former has the problem of low efficiency, the latter has the defect of huge expense and both techniques are difficult to be used on glass insulators [10,11].

Superhydrophobic (SHP) coatings based on the lotus leaf effect have excellent hydrophobic properties and are considered to be able to solve the problem of icing from the source, which has received extensive attention [12–14]. Under the action of micro–nano rough structures and low-surface-energy substances, the water droplets on the surface

of SHP coatings show Cassie state, which facilitates the rolling down of water droplets and reduces the possibility of freezing [15,16]. In addition, the rough structure of the SHP surface has a large air cushion, which decreases the solid–liquid contact area, effectively retards frosting and icing and also reduces the ice adhesion strength [17,18]. Xue et al. [19] prepared SHP anti-icing/deicing films by using laser etching. The combination of active heating eliminated the mechanical interlock between ice and the surface. The freezing time of water droplets on the surface of the MXene/PEI composite film was seven times longer than that of the untreated PEI film. Zhang et al. [20] fabricated SHP coatings with micropillar arrays by using network embossing and layer-by-layer assembly. The icing delay time was as high as 1750 s, and the average deicing shear force was reduced by 90% (about 0.31 N). Liu et al. [21] prepared SHP coatings using polysiloxane-modified SiO₂ particles compounded with fluorosilicone resin, showing excellent anti-icing properties in low-temperature environments. The complete icing time could be extended by 200% at −10 °C and 800% at −15 °C. Furthermore, the ice adhesion strength of the SHP coating was only 34 kPa. Chang et al. [22] successfully fabricated SHP PTFE/WO composite coatings through a combination of pulse electrochemical deposition and magnetron sputtering. The experimental results suggested that the SHP coating could significantly reduce the freezing temperature of water droplets, extend the freezing time, and exhibit good deicing performance (ice adhesion strength as low as 54.2 kPa). Pan et al. [23] found that SHP coatings of carbon fiber/epoxy composites prepared by combining spraying with hard-template hot-pressing displayed an icing delay time of up to 640 s and an ice adhesion strength as low as 50 kPa in −20 °C environments. Lei et al. [24–26] prepared SHP anti-icing coatings by using spraying, and the results showed that the SHP surface had excellent delayed icing performance and strong ability to inhibit frost growth. This implies that SHP coatings can be employed on insulators to prevent the occurrence of icing flashover. Although the SHP coatings prepared by using the above methods have excellent anti-icing properties, there are problems such as cumbersome processes and expensive equipment [19,21,22,27,28]. Therefore, the methods are difficult to apply to actual industrial production. As a simple and efficient technology, spraying can greatly decrease the cost of coating preparation, streamline the coating preparation process, and is widely used in the mass production of complex shaped parts [24–26,29–31]. However, most of the reports are based on metallic materials [20–22,25,26,31,32]. There are few studies on SHP anti-icing coatings for glass insulators. Furthermore, it has been demonstrated that high-density glaze icing is more harmful to glass insulators than frost and snow [33–35]. However, the current reports [19–22,25–28,31,32] are limited to simple surface frosting, water droplet freezing and ice adhesion strength tests. It is, therefore, worthwhile to investigate the anti-icing performance of SHP coatings in a glaze environment.

In this work, PTFE, Al₂O₃ and SiO₂ superhydrophobic coatings were successfully prepared on glass slides by using one-step spraying. The microstructure, three-dimensional structure and elemental composition of the coatings were characterized. The wettability, anti-icing and anti-glaze icing properties of the coatings were compared and analyzed. The surface of PTFE superhydrophobic coating had a uniformly distributed micro–nano structure, showing excellent hydrophobicity and anti-icing performance, meaning it has a good application prospect in the field of anti-icing of glass insulators. In addition, the anti-icing durability of the coatings under icing/melting, abrasion and UV tests was evaluated. After 20 icing/melting and 30 abrasion cycles, the wettability and anti-icing performance of the superhydrophobic coatings were somewhat degraded. However, the outstanding anti-icing performance could still be maintained after 624 h of UV irradiation.

2. Materials and Methods

2.1. Materials

Epoxy resin (GCC135) and curing agent were provided by Kunshan Lvixun Chemicals Industry Co., Ltd., Shanghai, China. Fluorosilicone resin was obtained from Chengdu Aikeda Chemical Reagent Co., Ltd., Chengdu, China. 1H, 1H, 2H, 2H heptadecafluorode-

cytrimethoxy silane (FAS-17) was supplied by Shanghai Aladdin Biochemical Technology Co., Ltd., Shanghai, China. Ethyl acetate was purchased from Chengdu Kelong Chemical Co., Ltd., Chengdu, China. Polytetrafluoroethylene (PTFE) with an average particle size of 200 nm, silicon dioxide (SiO₂) with an average particle size of 3–40 nm and alumina (Al₂O₃) with an average particle size of 30 nm were purchased from Shanghai Macklin Biochemical Co., Ltd., Shanghai, China. Glass slides (7101) were provided by Jiangsu Feizhou Glass Plastic Co., Ltd., Yixing, China. All reagents were used directly without further purification.

2.2. Preparation of Superhydrophobic Coatings

First, 25 g of ethyl acetate, 0.8 g of FAS-17 and nanoparticle powder were placed in a beaker. The mixed solution was subjected to magnetic stirring and ultrasonic dispersion for 10 min, respectively. Then, 4 g of epoxy resin and 3 g of fluorosilicone resin were added and magnetically stirred for 25 min. Finally, 1.2 g of epoxy resin curing agent was added and magnetically stirred for 10 min in order to fully mix the solution. The speed of magnetic stirring was 400 rpm. The coatings with different mass fractions were prepared by adding different masses of nanoparticles. Among them, the mass fractions of PTFE coating were 10%, 20%, 40%, 50% and 60%. For Al₂O₃ and SiO₂ coatings, the mass fractions were 5%, 10%, 20%, 40% and 50%, respectively. The well-mixed solution was poured into a spray bottle and sprayed against a vertically placed glass slide. The diameter of the nozzle was 1.5 mm, the spraying pressure was 0.3 MPa and the spraying distance was kept at 15 cm. In order to spray uniformly, the spray gun was moved slowly from top to bottom, and the spraying time was controlled at about 15 s. The sprayed specimens were cured at room temperature for half an hour and then placed in a vacuum drying oven overnight. During the curing process, the chemical bonding reactions occurred between the coating molecules sprayed onto the glass surface to form epoxidized amine. The epoxidized amine provided a strong bonding capability, which firmly bound the coating molecules to the glass through chemical bonding.

2.3. Characterization

The microscopic morphology and elemental composition of the coatings were characterized by using scanning electron microscopy (SEM, Zeiss Auriga) and energy dispersive spectrometer (EDS), respectively. To enhance the electrical conductivity for clear observation of the microstructure, a thin film of gold with a thickness of about 20 nm was applied to the surface of the coating using an ion sputterer. The three-dimensional morphology of the coatings was observed by using a laser scanning confocal microscope (LEXT OLS4000) and the roughness was measured. The contact angle (CA) and sliding angle (SA) of the coatings were measured by using a water contact angle measuring instrument (SINDIN SDC-100). The volume of the test water droplets was about 6 μ L. The measurements were repeated five times and averaged. A high-speed camera (M220, Revealer) was employed to evaluate the water droplet bouncing behavior of the coatings.

Water droplet freezing and ice adhesion strength tests were performed using a semiconductor refrigeration platform [8]. During the tests, the ambient temperature and humidity were controlled at 25 °C and 50%, respectively. First, 6 μ L of deionized water was dropped onto the coating surface. Next, the temperature of the cooling plate was lowered to -10 °C. Finally, a water contact angle measuring instrument was utilized to capture images of water droplets until they were completely frozen. The time from the start of the test to complete freezing was the freezing time. In addition, a cylindrical mold with an inner diameter of 10 mm was placed on the coating surface and filled with deionized water. The temperature of the cooling plate was set to -10 °C and maintained for more than 60 min to ensure complete freezing of the water inside the mold. The motion table was controlled to push off the mold from the coating surface. The force sensor recorded the peak force of the push-off. The ice adhesion strength was calculated from the peak force and the area of the cylindrical mold. Furthermore, the glaze icing test was carried out in the artificial climate chamber. The temperature in the climate chamber was maintained at -12 °C, the humidity

was 90° and the wind speed was 1.2 m/s. Water droplets with a diameter of 40 µm were sprayed on the surface of the specimens using a rain sprinkler. The inclination angle of the specimens was held at about 90°. The test lasted for a total of 80 min. The ice morphology of the specimens was photographed with a mobile phone camera at intervals. After the test, the icing weight was calculated according to the weight difference before and after the test.

The anti-icing durability of the coating was analyzed by using icing/melting, abrasion and UV tests. The icing/melting test was performed 20 times by controlling the temperature of the cooling plate to repeatedly freeze and melt. In addition, a 100 g weight was placed on the reverse side of the coating. Dragging the specimen to slide on 400# sandpaper for 5 cm was recorded as one abrasion. The contact angle, sliding angle and ice adhesion strength of the coating were measured after every five abrasion cycles. A total of 30 abrasion cycles were conducted. Referring to the standard IEC-61109-2008, the UV irradiation test was carried out in a KW-UV3 ultraviolet aging test chamber. The light source was a 500 W high-pressure mercury lamp with a UV radiation intensity of 162.5 W/m² and a wavelength of 365 nm. The specimen was fixed at a distance of 10 cm from the UV lamp, and the test temperature was 50 °C. After every 48 h of irradiation, the contact angle and sliding angle of the coating were measured. At the end of the test, the ice adhesion strength of the coating was measured.

3. Results and Discussion

3.1. Microscopic Morphology

The microscopic morphology of the coatings with different mass fractions is shown in Figure 1. The yellow dashed lines in the figure denote micron-scale structures. When the PTFE mass fraction is 10%, the surface of the specimen is relatively smooth, and the laminated structure appears in the local area. With the increase in PTFE mass fraction, a rough structure is formed on the surface. The PTFE nanoparticles are gradually constructing micrometer-scale protruding structures. The surface of the specimen with a mass fraction of 40% becomes inhomogeneous, and a rough structure consisting of protrusions, pits and PTFE particles is observed. When the mass fraction is increased to 50%, the surface of the specimen has the flattest rough structure with nanosized PTFE particles all over the entire surface. It is noteworthy that the nanoparticles on the surface of the specimen with a mass fraction of 60% undergo agglomeration and are embedded in the binder composed of epoxy and fluorosilicone resins. This implies that there is a significant effect of PTFE particles on the microstructure of the coating (Figure 1a). In addition, the influences of Al₂O₃ and SiO₂ nanoparticles are also compared. When the mass fraction of Al₂O₃ and SiO₂ coatings is 5%, sporadically distributed nanostructures emerge on the surface of the specimens. The Al₂O₃ and SiO₂ nanoparticles are wrapped around each other by epoxy resin to create micrometer-scale block structures. As the mass fraction of Al₂O₃ and SiO₂ increases, the micro–nano structures on the surface gradually increase. The specimen with 40% mass fraction has a relatively flat and rough structure with nanoparticles distributed over the entire surface (Figure 1b,c). When the mass fraction continues to increase to 50%, a large number of holes appear on the surface of the specimen. Compared with Al₂O₃ and SiO₂ coatings with a mass fraction of 40%, the PTFE coating with a mass fraction of 50% has a denser and more uniform micro–nano structure. Therefore, the rough surface with micro–nano structures can be prepared by using spraying. However, the reasonable addition of the appropriate amount of nanoparticles is a prerequisite for producing a homogeneous structure. On the other hand, the thicknesses of PTFE (50%), Al₂O₃ (40%) and SiO₂ (40%) coatings, measured by using a micrometer, were 160, 93 and 87 µm, respectively. This is because the PTFE nanoparticles are easier to mix with the binder, which facilitates spraying.

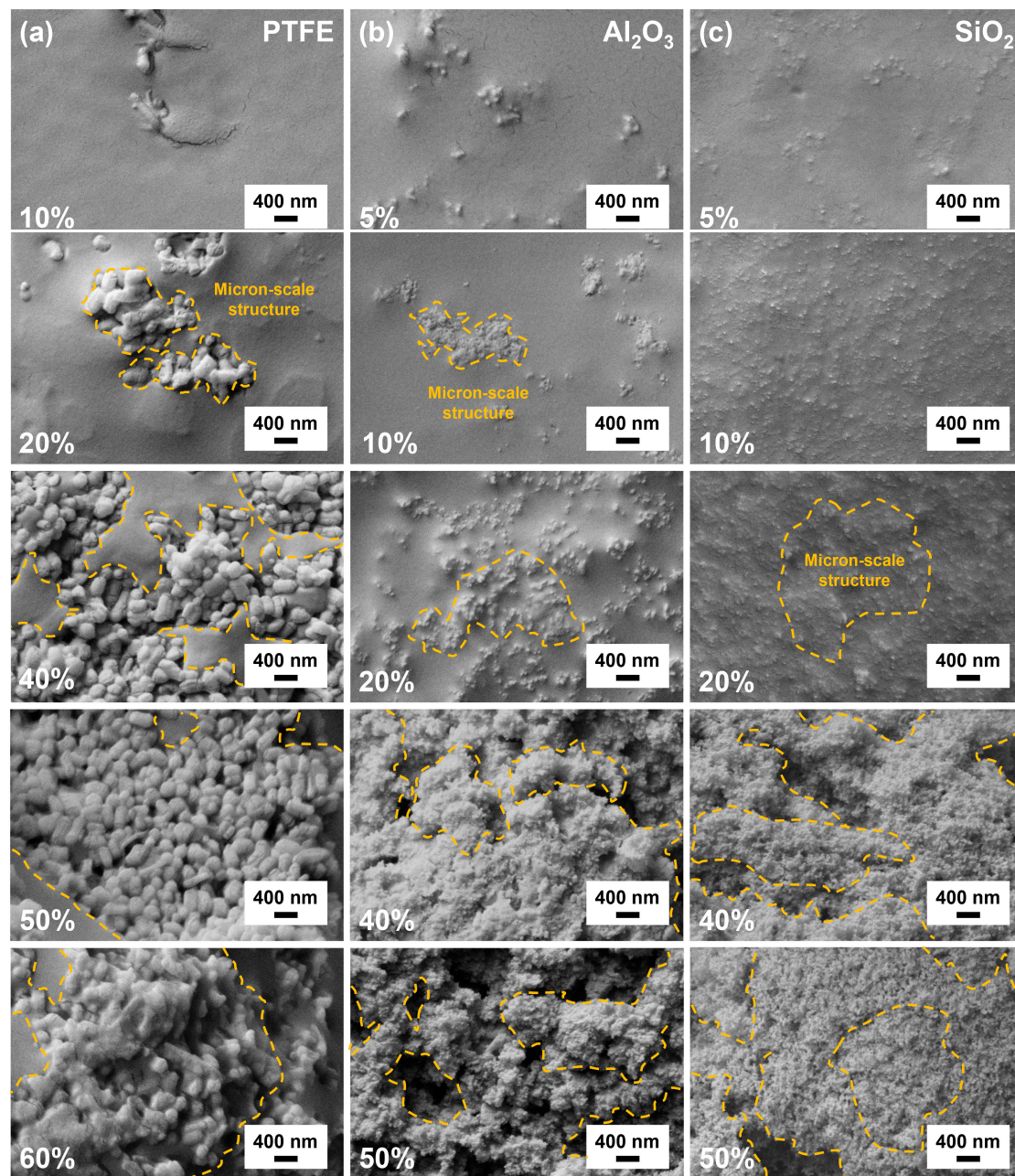


Figure 1. Microscopic morphology of PTFE (a), Al_2O_3 (b) and SiO_2 (c) coatings.

The three-dimensional morphology and surface roughness of the coatings with different mass fractions are presented in Figure 2. When fewer nanoparticles are added, the surface of the specimen has fewer protruding structures and most of the area maintains a smooth morphology. With the increase in nanoparticle content, the granular structure on the surface increases. At this time, dense protruding structures appear on the surface of the specimen and the surface roughness gradually increases, which coincides with the SEM results (Figure 1). This indicates that the increase in nanoparticle content contributes to the formation of rough structures. It can also be found from Figure 2 that coatings prepared by using spraying tend to form micrometer-scale protruding structures. This is attributed to the special process of spraying, similar to that reported by Fan et al. [14,25,26]. Before spraying, ethyl acetate was added as a solvent to mix the nanoparticles, epoxy resin and fluorosilicone resin. Due to the easy evaporation property of ethyl acetate, the amount of ethyl acetate is rapidly reduced when the mixed solution is sprayed onto the

glass surface under the action of an air compressor. During the rapid evaporation of the solvent, the nanoparticles and the binder crosslink with each other, leading to the formation of protruding structures. In addition, the strong airflow generated by the air compressor accelerates the solvent evaporation and solution curing, which, in turn, also promotes the generation of protruding structures. The micron-scale and nanoscale rough structures are necessary conditions for achieving superhydrophobicity [15–18]. The presence of nanoscale structures is confirmed by the large number of PTFE, Al₂O₃ and SiO₂ nanoparticles on the surface (Figure 1). Additionally, the microscopic morphology, three-dimensional structure and micrometer-scale surface roughness indicate the formation of micron-scale structures (Figures 1 and 2). Therefore, the binary micro–nano structures can be sprayed with reasonable addition of nanoparticles, which is favorable for the preparation of superhydrophobic coatings.

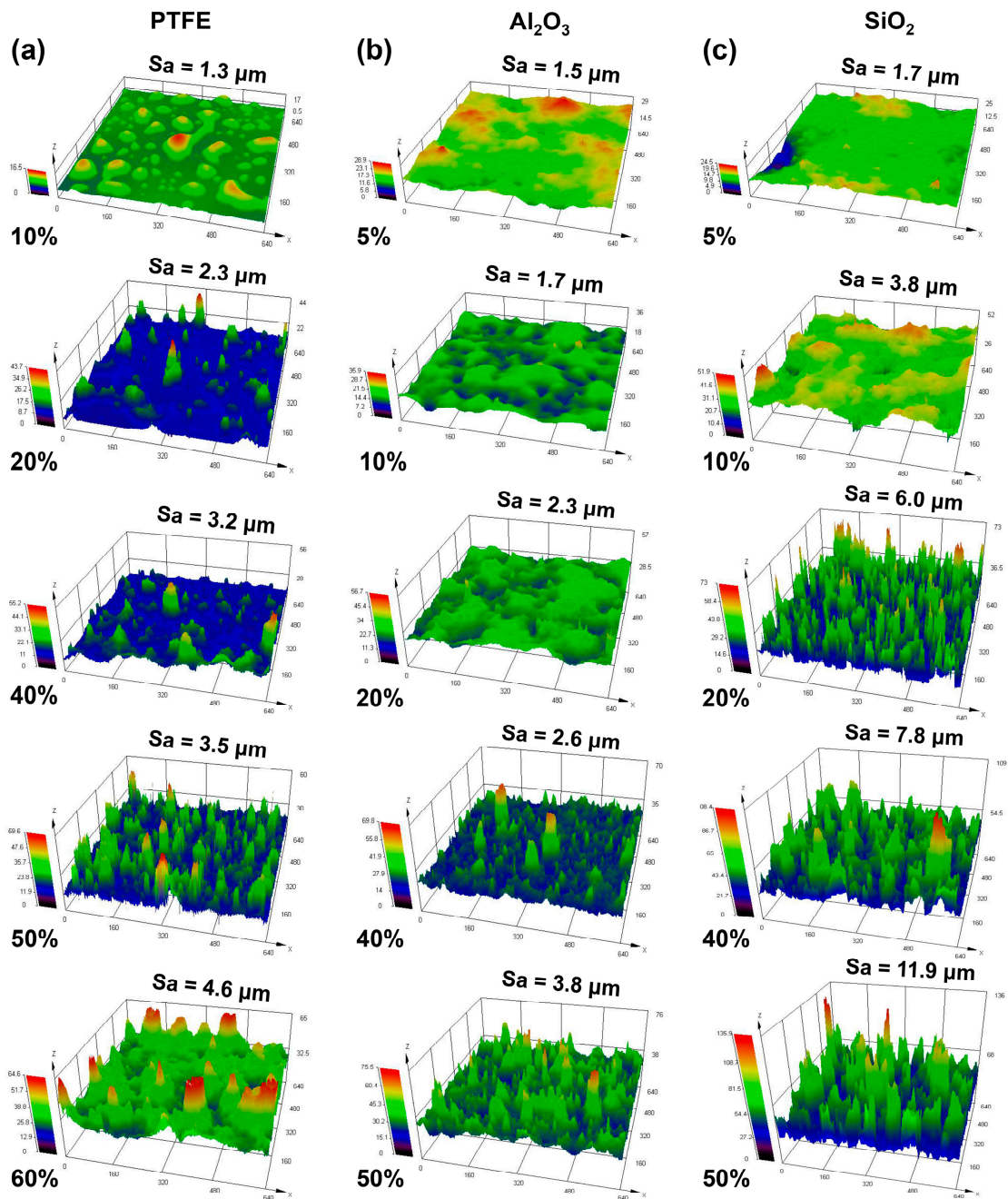


Figure 2. Three-dimensional morphology of PTFE (a), Al₂O₃ (b) and SiO₂ (c) coatings.

The elemental composition on the surface of the three coatings is displayed in Figure 3. For the PTFE coating with 50% mass fraction, a large amount of F element is distributed on the surface, and the F element content is as high as 42.77% (Figure 3a). This is due to the large number of C–F bonds brought about by the addition of fluorosilicone resin, FAS-17 and PTFE particles, indicating that the PTFE particles and fluorosilicone resin can be uniformly sprayed onto the surface of the specimen. Furthermore, PTFE nanoparticles enriched with C–F bonds not only construct the rough structure on the surface but also reduce the surface energy, which is conducive to the improvement of hydrophobic properties [36,37]. Figure 3b illustrates that there are many Al elements on the surface of the Al₂O₃ coating, which is because the Al₂O₃ particles contain a large amount of Al. On the other hand, the surface of the SiO₂ coating is covered with uniform SiO₂ particles, which are tested to have a high content of Si elements (Figure 3c). Compared with Al₂O₃ and SiO₂ coatings, the PTFE coating with a high content of F elements is the easiest to realize superhydrophobic properties.

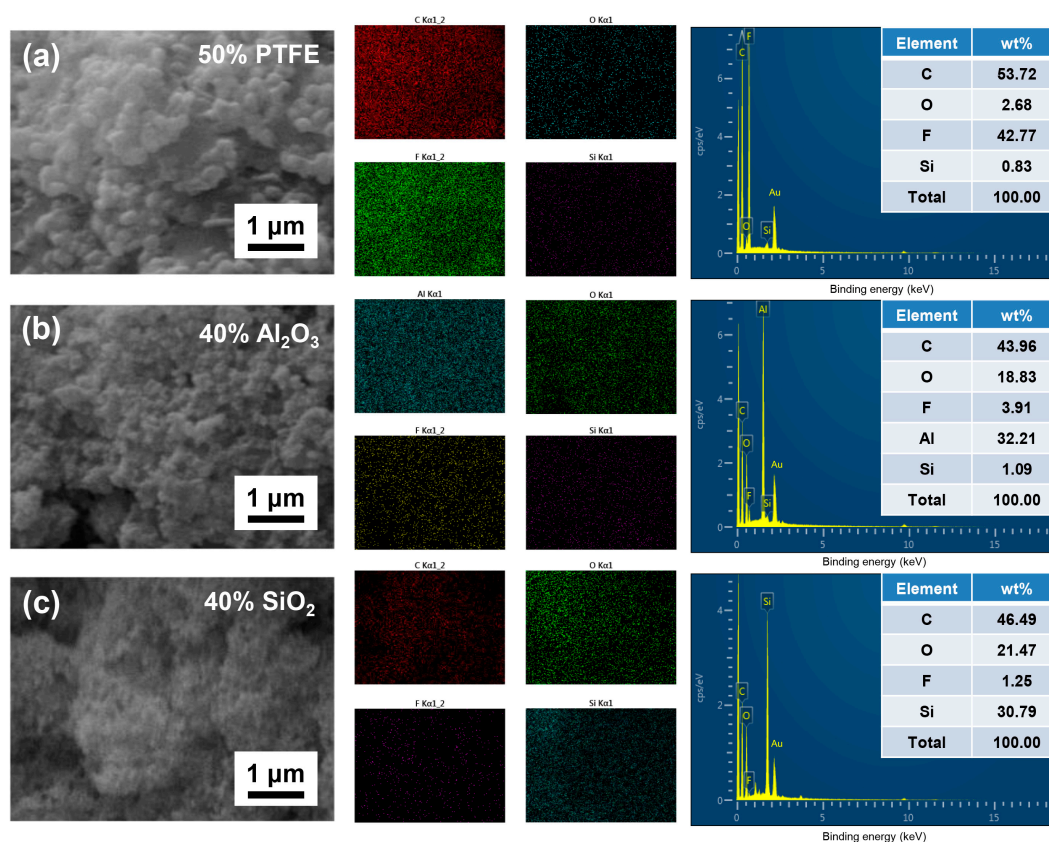


Figure 3. Elemental composition on the surface of PTFE (a), Al₂O₃ (b) and SiO₂ (c) coatings.

3.2. Wettability

The contact angle and sliding angle of the coatings with different mass fractions are shown in Figure 4. The contact angles of all coatings are significantly enhanced as compared to glass (42.6°). The PTFE coatings with mass fractions of 50% and 60% have similar contact angles, which are as high as 165.5° and 166.0°, respectively. The contact angles of Al₂O₃ and SiO₂ coatings with mass fractions of 40% and 50% are relatively close. The former are 160.5° and 159.9°, and the latter are 161.0° and 161.7°, respectively. Moreover, the sliding angle is utilized to evaluate the water droplet sliding performance on the surface of the three coatings. The sliding angles of the specimens exhibit a trend of rapid decrease followed by some increase as the mass fraction increases. The PTFE coating with a mass fraction of 50% has a sliding angle as low as 3.1°. The sliding angles of the Al₂O₃ and SiO₂ coatings with a mass fraction of 40% are 1.3° and 2.1°, respectively. Therefore, according to the

definition of superhydrophobicity [38,39], the PTFE coating with 50% mass fraction and the Al_2O_3 and SiO_2 coatings with 40% mass fraction all meet the criteria of superhydrophobic materials. With the gradual increase in added nanoparticles, a certain micro–nano rough structure is formed on the surface of the specimen (Figures 1 and 2). In this case, the water droplets can be supported by the air cushion in the rough structure to assume the Cassie state, and the coating exhibits a contact angle higher than 160° and a sliding angle lower than 5° . Therefore, it is easy for the water droplets to leave the surface before freezing, which improves the possibility of applying superhydrophobic coatings for anti-icing. Additionally, it is noted that for superhydrophobic surfaces, the PTFE coating has a slightly higher contact angle than the Al_2O_3 and SiO_2 coatings. However, the sliding angle of the former is greater than the latter two. This is due to the uneven micro–nano structures on the surface of the Al_2O_3 and SiO_2 coatings (Figures 1 and 2), which make it difficult for the water droplets to be placed stably on the surface and mean the droplets exhibit a tendency to roll away more easily (effectively reducing the sliding angle). Meanwhile, the more homogeneous micro–nano structure on the surface of the PTFE coating leads to the water droplets remaining in a stable Cassie state, thereby measuring a higher contact angle.

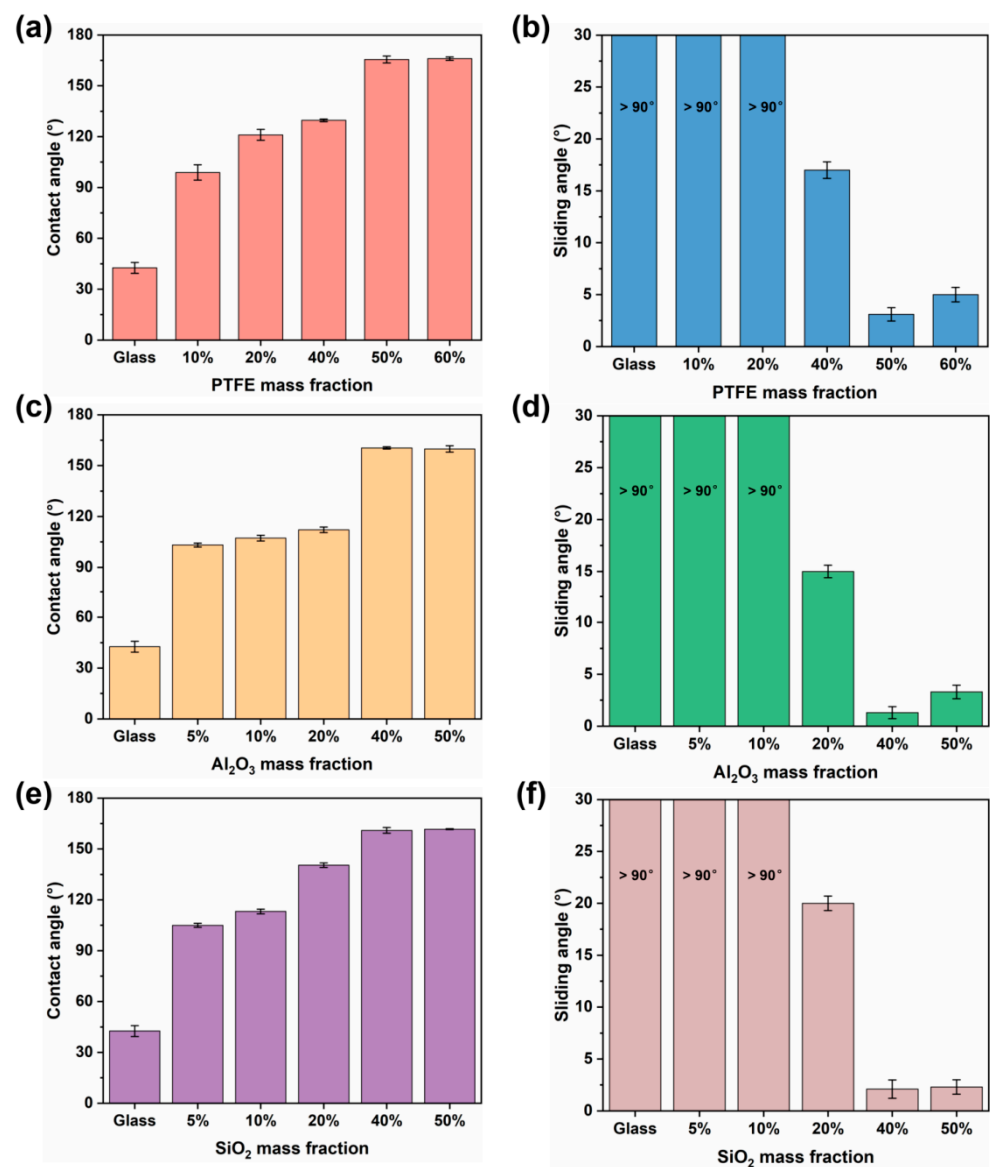


Figure 4. Contact angle (a,c,e) and sliding angle (b,d,f) of the three coatings.

A high-speed camera was used to analyze the water droplet bouncing behavior on the surface of three superhydrophobic coatings (PTFE coating with 50% mass fraction, Al_2O_3 and SiO_2 coatings with 40% mass fraction), and the results are presented in Figure 5. Figure 5a illustrates a schematic diagram of a water droplet bouncing. It is obvious that the water droplet after impacting the glass adheres to the surface and finally assumes the shape of a hydrophilic ellipsoid (Figure 5b). In contrast, the water droplet rebounds several times after impacting the surface of the three superhydrophobic coatings. The enlarged image of the water droplet bouncing also indicates that the water droplets on the surface of the superhydrophobic coatings have distinct signs of rebounding. Compared with the water droplet rebounding two times on the surface of Al_2O_3 and SiO_2 coatings, the water droplet on the surface of PTFE coating can rebound five times (Figure 5c–e). In addition, the rebound height of water droplet on the surface of PTFE coating is dramatically higher than that of Al_2O_3 and SiO_2 coatings. This suggests that the energy dissipation induced by adhesion on the surface of the PTFE coating is small, retaining enough energy for the water droplet to bounce away repeatedly [40,41]. Therefore, due to the uniform rough structure and low surface energy substances (Figures 1–3), the PTFE coating exhibits excellent water droplet bouncing performance, which is beneficial to the water droplet bouncing away, reducing the water droplet contact time and the possibility of icing [42].

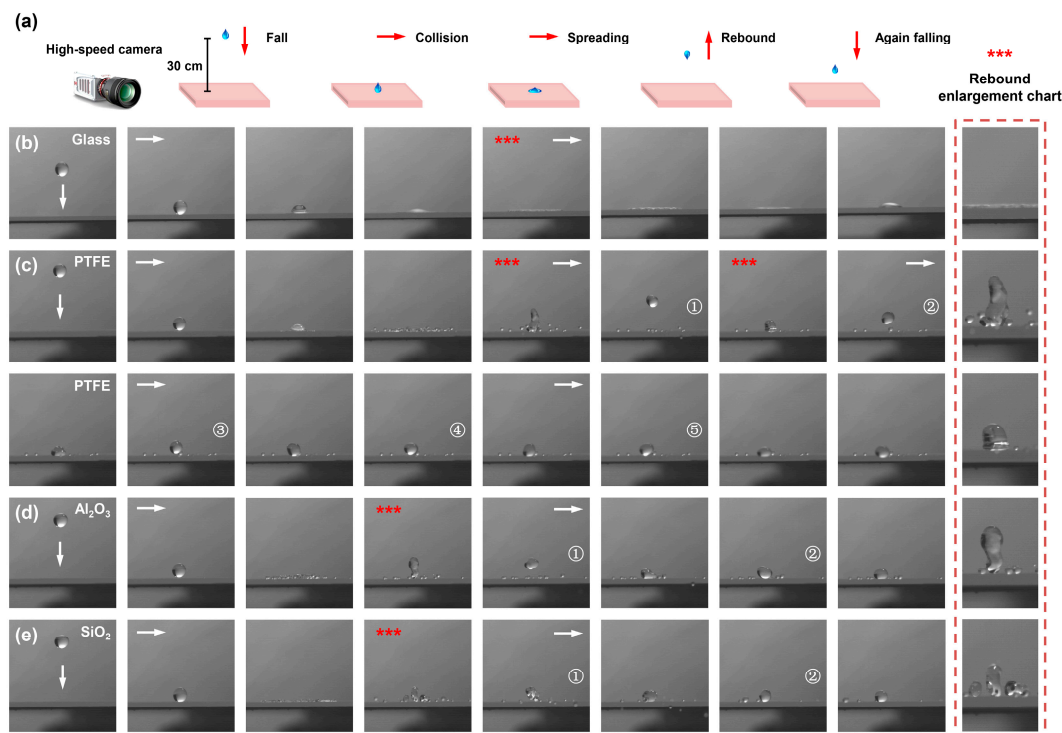


Figure 5. Water droplet bouncing schematic (a), water droplet bouncing behavior on the surface of glass (b) and three superhydrophobic coatings (c–e). *** indicates an enlarged view of a water droplet bouncing (the rightmost dotted box). ①–⑤ denote the number of successful bounces of the water droplet.

Due to the volatilization of the solvent and the crosslinking curing of the epoxy resin, the micro–nano structures can be fabricated on glass by using spraying [14,25,26,37]. Different kinds of nanoparticles were added to form different types of rough structures [25,26,37]. The PTFE coating surface is distributed with homogeneous nanoparticles, which creates protruding micro–nano structures (Figure 1a). The Al_2O_3 and SiO_2 coating surfaces are characterized by the formation of blocky micro–nano structures consisting of nanoparticles (Figure 1b,c). From the three-dimensional structures, there are obvious micrometer-scale protruding structures on the three coating surfaces (Figure 2). The measured surface rough-

ness ($>1.3 \mu\text{m}$) also verifies the micrometer-scale structure. Therefore, the constructed micro–nano structures and low-surface-energy substances (Figure 3) enable all three coatings to realize excellent superhydrophobicity (Figure 4). However, the influence law of hydrophobicity of the PTFE, Al_2O_3 and SiO_2 coatings is further analyzed from different scales. On the nanoscale, the nanoparticles are often the key to achieve superhydrophobicity [14,42]. Dense nanoparticles appear on the surface of the three coatings (Figure 1), which exhibit a contact angle higher than 160° and a sliding angle lower than 5° (Figure 4). This implies that the effect of nanoparticles on the hydrophobicity of the coatings is similar. The hydrophobicity is improved by building up a micrometer-scale structure and reducing the surface energy [15,37]. Interestingly, the water droplet bouncing performance of the PTFE coating is significantly better than that of the Al_2O_3 and SiO_2 coatings. This is related to the micron-scale structure on the surface. Compared with the pitted micrometer-scale protruding structures on the surface of the Al_2O_3 and SiO_2 coatings, the PTFE coating has a more uniform micrometer-scale structure (Figures 1 and 2). As a result, the water droplets are more easily dispersed upon impact with the Al_2O_3 and SiO_2 coating surfaces, forming multiple small droplets (Figure 5d,e). At this point, the water droplets lose more energy and cannot rebound repeatedly. In contrast, the water droplets dispersed after impact on the PTFE coating surface are smaller (Figure 5c), retaining enough energy to repeat the rebound five times, presenting excellent water droplet bouncing performance. In summary, it is necessary to consider the relationship between the rough structure and hydrophobicity of the superhydrophobic coating from the micro and nano scales, so as to guide the subsequent preparation of the superhydrophobic coating.

3.3. Anti-Icing Properties

The water droplet freezing test was performed on glass and three superhydrophobic coatings. Figure 6a illustrates the freezing process of water droplet on the surface. Under the continuous action of the refrigeration platform, the water droplet on the surface is gradually cooled and frozen. In general, the water droplet is more prone to the freezing behavior of heterogeneous nucleation because the energy barrier of heterogeneous nucleation is lower than that of homogeneous nucleation [43]. As a result, the transparent water droplet is transformed into an opaque frozen state during the heterogeneous nucleation process. Similar to the results of water droplet bouncing (Figure 5), the completely frozen water droplet almost spreads on the surface of glass. However, the water droplet on the surface of the three superhydrophobic coatings shows a spheroidal shape. Furthermore, the freezing time of the water droplet on the surface of the glass and the three superhydrophobic coatings was measured, as displayed in Figure 6b. The glass has the shortest freezing time of 291.2 s. The PTFE coating has the highest freezing time of 4898.7 s, which is more than 16 times that of the glass. The freezing times of Al_2O_3 and SiO_2 coatings are also improved, reaching 2488.4 and 1694.5 s, respectively. This is owing to the micro–nano rough structures on the surface of the three superhydrophobic coatings (Figures 1 and 2). The water droplet on the surface of superhydrophobic coating can keep Cassie state, which reduces the solid–liquid contact area. It is well known that air is a poor conductor of heat. The large number of air cushions in the rough structure greatly decreases the heat transfer efficiency and effectively retards the freezing of water droplet [44,45]. Notably, the PTFE coating exhibits a much higher freezing time than the Al_2O_3 and SiO_2 coatings. This is mainly due to the more uniform rough structure (Figure 1) and large number of C–F bonds on the PTFE coating surface. The uniform rough structure on the surface can maximize the effect of the air cushion on decreasing the heat transfer rate, which effectively retards icing. The Al_2O_3 and SiO_2 coating surfaces present a distinct micrometer-scale protruding structure (Figures 1 and 2). Furthermore, it has been reported that the surface energy of PTFE nanoparticles is lower than that of Al_2O_3 and SiO_2 nanoparticles [46–48]. Therefore, both the protruding structures and nanoparticles on the surface of the Al_2O_3 and SiO_2 coatings may act as nucleation points for the freezing of water droplets, which accelerates icing. On the other hand, the high amount of F elements detected on the surface (Figure 3)

confirms the presence of a large number of C–F bonds on the surface of the PTFE coating, which can significantly reduce the surface energy. The surface with low surface energy can also delay the freezing of water droplets. In conclusion, under the synergistic effect of homogeneous micro–nano structures and surface-dispersed C–F bonds, the PTFE coating has the best performance in delaying freezing compared to the Al₂O₃ and SiO₂ coatings.

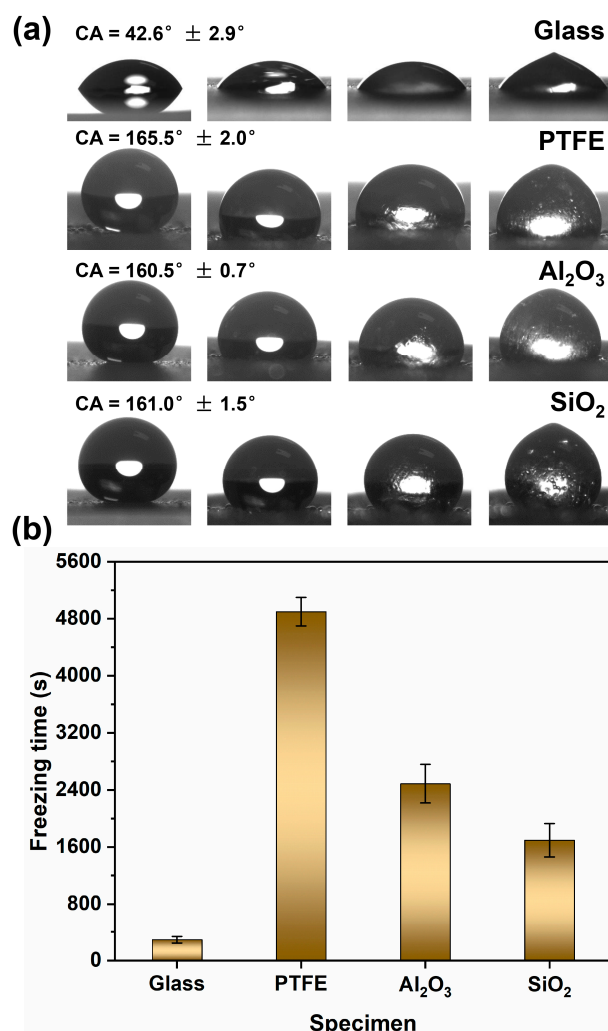


Figure 6. Freezing process (a) and freezing time (b) of water droplet on glass and three superhydrophobic coatings.

Numerous studies have demonstrated that superhydrophobic surfaces can significantly delay frosting and icing [14,17,49]. However, the occurrence of icing cannot be avoided in the harsh low-temperature environment for a long time. At this point, the icephobic properties of superhydrophobic surfaces should be improved and the ice adhesion strength should be reduced, to facilitate timely deicing after icing. The ice adhesion strength of glass and three superhydrophobic coatings was measured, and the results are shown in Figure 7. The schematic diagram of the ice adhesion strength test is also given in the figure. Coinciding with the freezing time (Figure 6), the glass exhibits the highest ice adhesion strength (255.1 kPa). The ice adhesion strength of the three superhydrophobic coatings is obviously reduced, reaching the criterion of less than 100 kPa for icephobic materials [50]. Among them, the ice adhesion strength of the PTFE coating is only 27.5 kPa, which is more than nine times lower than that of glass. The ice adhesion strengths of Al₂O₃ and SiO₂ coatings are increased to 61.1 and 89.8 kPa, respectively. It can be noted that the ice adhesion strength of PTFE coating is lower than Al₂O₃ and SiO₂ coatings,

which is attributed to the micro–nano structure of the coating. The surface of the PTFE coating has the flattest rough structures, whereas the microstructures of the Al_2O_3 and SiO_2 coatings are observed to have a higher number of pore defects (Figure 1). Therefore, the supercooled water may infiltrate into the holes when icing occurs, allowing the ice to form a mechanical interlock with the holes, which, in turn, leads to a higher ice adhesion strength [51]. In addition, low-surface-energy substances reduce ice adhesion strength by decreasing van der Waals and electrostatic forces [52,53]. A high content of F element is detected on the surface of PTFE coating (Figure 3), suggesting that the presence of a large amount of low-surface-energy substances also favors the reduction in ice adhesion strength. In summary, the PTFE coating shows excellent icephobic properties, which is favorable for the effective deicing of insulators after ice-covering.

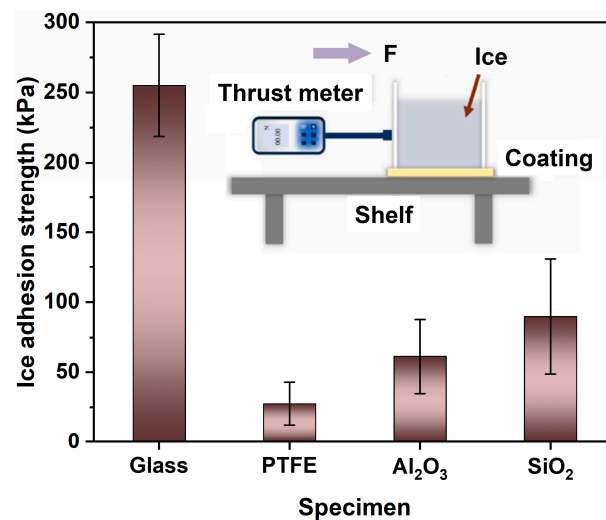


Figure 7. Ice adhesion strength of glass and three superhydrophobic coatings.

The anti-glaze icing properties of glass and three superhydrophobic coatings were evaluated in an artificial climate chamber, as presented in Figure 8. The surface of the glass starts to be covered with ice at 25 min. There are many frozen water droplets on the surface. At this time, the surface of the three superhydrophobic coatings still maintains good hydrophobicity, and only a small number of water droplets are observed in the uncoated areas (edges and behind). As the time extends to 50 min, the surface of the glass is covered with a completely frozen ice layer, and obvious icicles are formed under the specimen. It can be seen that the surface of the three superhydrophobic coatings exhibits the freezing of water droplets. However, the surface preserves an almost complete area of uncoated ice. When the time is 80 min, the ice layer on the surface of the glass becomes thicker and the icicles also grow significantly. Although the ice-covered area on the surface of the three superhydrophobic coatings has increased, there are still large areas without icing. Here, it should be explained that the surrounding and back of the glass slide are uncoated areas, which are as susceptible to icing as glass, resulting in icicles on the lower part and back of the three superhydrophobic coatings. Excluding these uncoated areas, the three superhydrophobic coatings have a large number of uniced areas on the front side. Compared with glass, the three superhydrophobic coatings show excellent glaze icing resistance. This is attributed to the fact that the excellent superhydrophobicity allows water droplets to roll away from the surface very easily, dramatically reducing the contact time and freezing possibility of water droplets.

Figure 9 displays the glaze icing weight of glass and three superhydrophobic coatings. In comparison to the icing weight of glass (2.02 g), the icing weight of the three superhydrophobic coatings is greatly decreased. The icing weights of SiO_2 , Al_2O_3 and PTFE coatings reduce to 1.78, 1.84 and 1.38 g, respectively. In particular, the icing weight of PTFE

coating is about 32% lower than that of glass. Therefore, the PTFE coating exhibits excellent resistance to glaze icing, effectively delaying glaze icing and reducing icing weight.

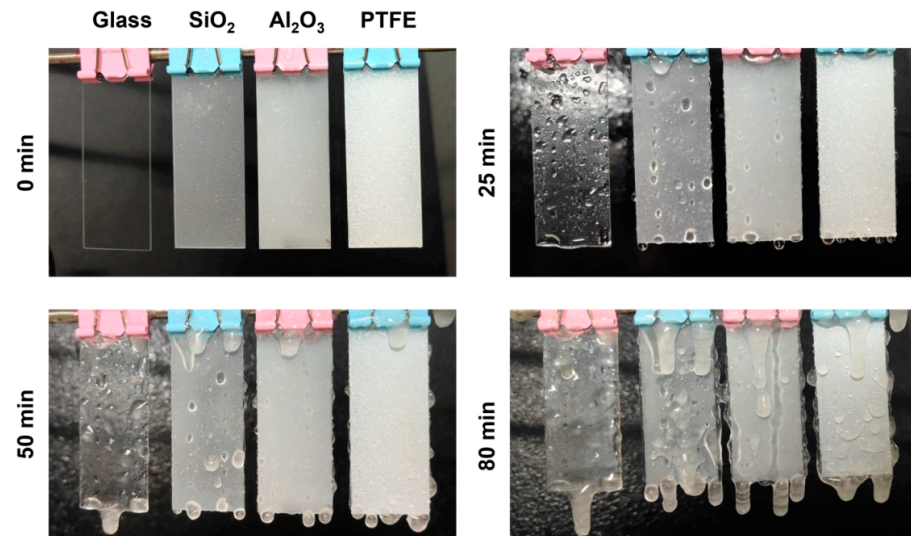


Figure 8. Glaze icing process of glass and three superhydrophobic coatings.

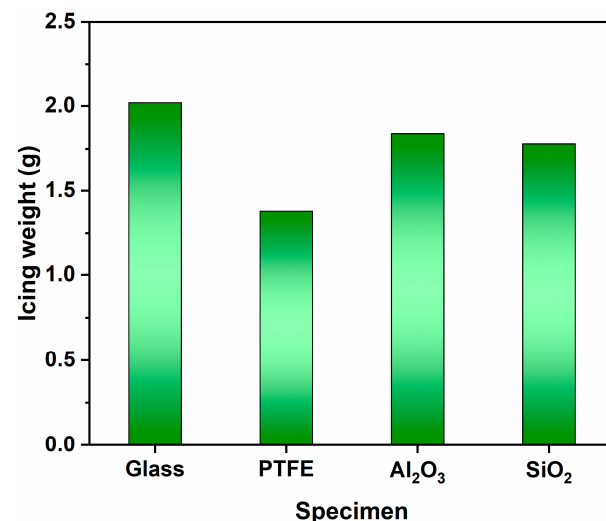


Figure 9. Glaze icing weight of glass and three superhydrophobic coatings.

It is well known that surface free energy, adhesion work and superhydrophobicity are closely related. In general, the lower the surface free energy, the better the hydrophobicity [14,54,55]. On the other hand, the surface adhesion work is inversely related to the contact angle [54]. Compared with the surface free energy of glass, which is as high as 41.94 mJ/m² [54], the surface free energy of the added fluorosilicone resin is around 23.0–24.2 mJ/m² [56]. In addition, the surface free energies of PTFE and SiO₂ particles were reported to be 18.7 and 34.18 mJ/m², respectively [46,48], whereas the surface free energy of Al₂O₃ particles was around 31.36–49.12 mJ/m² [47]. The above surface free energy data are in agreement with the wettability results (Figures 4 and 5). The surface of the PTFE coating has the lowest surface free energy (Figure 3), showing a better contact angle (Figure 4) and anti-icing properties (Figures 6 and 7) than the Al₂O₃ and SiO₂ coatings. Furthermore, the highest contact angle results in the lowest work of adhesion on the surface of the PTFE coating, which facilitates the roll-off of water droplets from the surface and thus improves the anti-icing properties (Figures 6–9). To summarize, the selection of nanoparticles and modifiers with low surface free energy can further enhance

the hydrophobicity and anti-icing performance of the coating. Optimizing the formulation design between nanoparticles and modifiers can provide guidance for the preparation of superhydrophobic anti-icing coatings.

3.4. Durability

To evaluate the anti-icing durability of superhydrophobic coating, the PTFE coating was selected for the icing/melting test. The wettability, ice adhesion strength, microscopic morphology and elemental composition of the coating after 20 icing/melting cycles were characterized, as shown in Figure 10. A schematic diagram of the icing/melting test is illustrated in Figure 10a. As the number of icing/melting cycles increases, the contact angle of the coating decreases slowly and the sliding angle increases gradually. Similar to the variation trend of the sliding angle, the ice adhesion strength of the coating gradually increases with the number of icing/melting cycles. After 20 icing/melting cycles, the contact angle of the coating decreases to 149.2° and the sliding angle increases to 13.8° (Figure 10b). The ice adhesion strength of the coating is increased to 53.8 kPa (Figure 10c). It can be seen from Figure 10d that the microstructure of the coating is not damaged by icing/melting. There are still micro-nano rough structures on the surface. However, after 20 icing/melting cycles, the F element content on the coating surface decreases from the initial 42.77% to 37.52% (Figure 10e). This indicates that the low-surface-energy substances on the coating surface decrease with the increase in the number of icing/melting cycles. Therefore, the hydrophobicity and anti-icing performance of the superhydrophobic coating will gradually degrade with continuous icing/melting cycles.

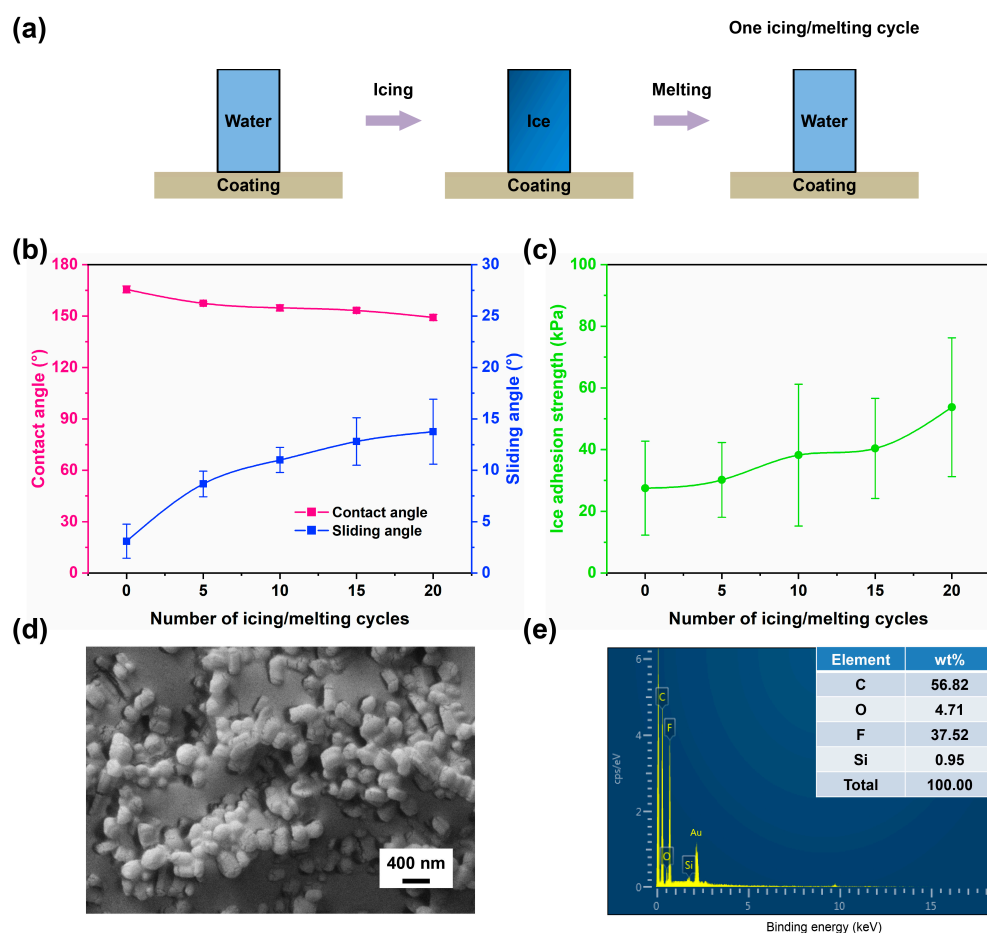


Figure 10. Schematic of icing/melting test (a), wettability (b), ice adhesion strength (c), microscopic morphology (d) and elemental composition (e) of PTFE superhydrophobic coating after 20 icing/melting cycles.

Most of the currently reported superhydrophobic coatings are relatively fragile, and even slight abrasion and vibration may lead to the loss of superhydrophobic properties [57–59]. This seriously limits their application in industrial production and daily life. Therefore, the abrasion durability of PTFE coating was explored, as illustrated in Figure 11. Figure 11a represents a schematic diagram of the abrasion test. Unlike the icing/melting test (Figure 10b), the effect of abrasion on the wettability of the coating is more severe. With increasing number of abrasion cycles, the contact angle of the coating decreases slowly, while the sliding angle increases rapidly. After 30 abrasion cycles, the contact angle of the coating decreases to 148.3° and the sliding angle increases to 35.7° (Figure 11b). In addition, the ice adhesion strength of the coating gradually increases to 74.5 kPa as the number of abrasion cycles increases (Figure 11c). It can be found that abrasion remarkably destroys the micro–nano structure of the coating. The nanoparticles on the surface of the coating are seriously scratched, showing scratches along the direction of abrasion (Figure 11d). At the same time, the F element content on the surface of the coating also decreases substantially to 34.23% (Figure 11e). Therefore, the damage of abrasion to the anti-icing performance of the superhydrophobic coating is more significant. It is necessary to further design the combination of binder and nanoparticles to enhance the abrasion durability of micro–nano structures.

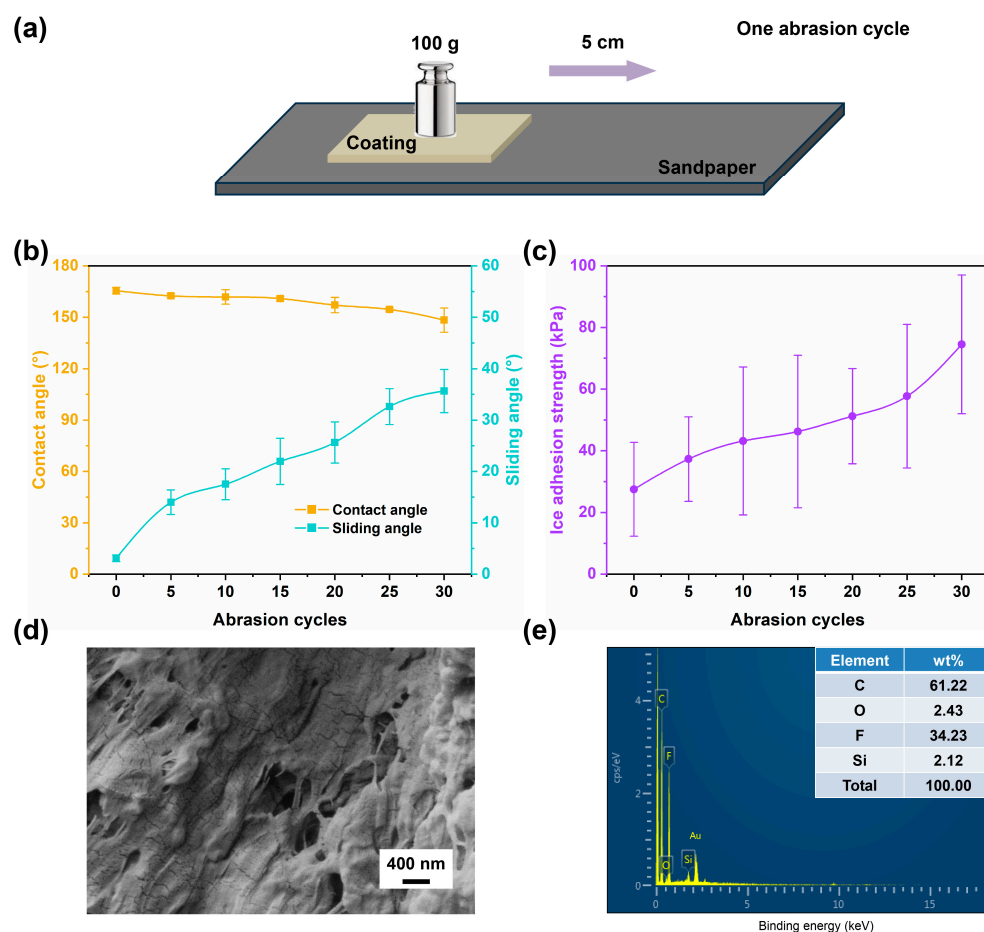


Figure 11. Schematic of abrasion test (a), wettability (b), ice adhesion strength (c), microscopic morphology (d) and elemental composition (e) of PTFE superhydrophobic coating after 30 abrasion cycles.

It is inevitable that glass insulators in long-term service will be affected by sunlight. To investigate the anti-icing durability of superhydrophobic coating under prolonged UV irradiation, the PTFE coating was subjected to UV testing, and the results are displayed in

Figure 12. Figure 12a depicts a schematic diagram of the UV irradiation test. After 624 h of UV radiation testing, the contact angle and sliding angle of the coating show less variation. The contact angle is maintained above 150° and the sliding angle remains in the range of $3\text{--}5^\circ$ (Figure 12b). Compared with the initial coating (27.5 kPa), the ice adhesion strength of the coating is only slightly increased to 30.5 kPa after UV radiation (Figure 12c). Furthermore, the microscopic morphology (Figure 12d) and elemental composition (Figure 12e) also suggest that the effect of long-term UV irradiation on the micro–nano rough structure and low-surface-energy substances of the coating is almost negligible. Therefore, the superhydrophobic coating prepared in this work can still maintain excellent superhydrophobic and anti-icing properties after UV radiation aging for up to 624 h, exhibiting outstanding potential for outdoor applications.

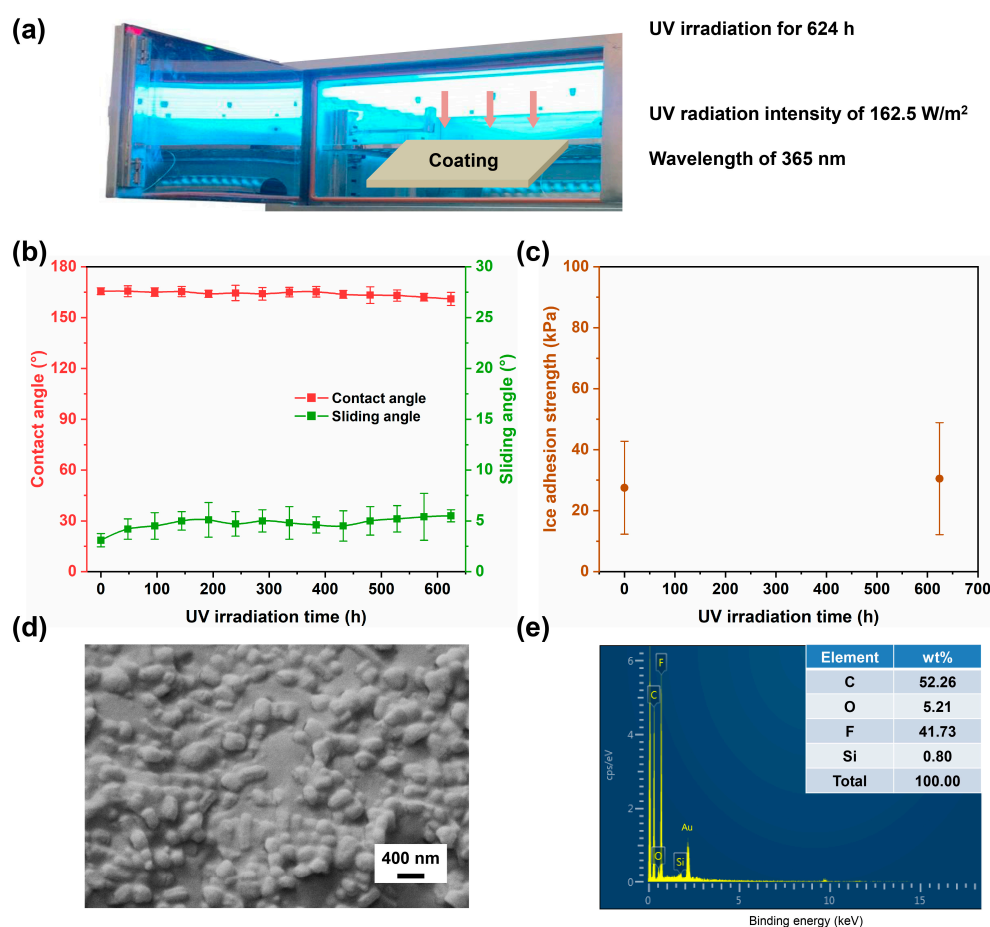


Figure 12. Schematic of UV irradiation (a), wettability (b), ice adhesion strength (c), microscopic morphology (d) and elemental composition (e) of PTFE superhydrophobic coating after UV irradiation for 624 h.

4. Conclusions

The microstructure, wettability, anti-icing and anti-glazing properties of PTFE, Al₂O₃ and SiO₂ superhydrophobic coatings prepared by using one-step spraying were investigated. Compared with Al₂O₃ and SiO₂ coatings, PTFE superhydrophobic coating had a more uniform rough structure, and the surface contained a high content of low-surface-energy substances. A contact angle of up to 165.5° and a sliding angle as low as 3.1° were measured for the PTFE superhydrophobic coating, which facilitated the bouncing of water droplets off the surface up to five times, reducing the potential of freezing. The anti-icing test results showed that the PTFE superhydrophobic coating not only extended the freezing time to 4898.7 s (more than 16 times beyond that of glass) but also reduced the ice adhesion

strength to 27.5 kPa (more than 9 times below that of glass). After 80 min of glaze icing, the surface of the glass was completely covered with a thick layer of ice. However, there were still large uniced areas on the surface of PTFE superhydrophobic coating, and its icing weight (1.38 g) was about 32% lower than that of glass. The hydrophobicity and anti-icing performance of the PTFE superhydrophobic coating decreased after 20 icing/melting cycles and 30 abrasion cycles, which was attributed to the loss of low-surface-energy substances and the destruction of the rough structure. It should be emphasized that the PTFE superhydrophobic coating maintained a contact angle of more than 150°, a sliding angle of less than 5° and an ice adhesion strength of 30.5 kPa after UV irradiation of up to 624 h. In summary, the superhydrophobic coatings prepared in this work have excellent anti-icing, icephobic and anti-glaze icing properties, which improves the possibility of practical application of anti-icing coatings. Subsequent research should focus on the matching of binders and nanoparticles to further enhance the mechanical durability of superhydrophobic coatings.

Author Contributions: Conceptualization, L.F., M.X., J.L., B.L. and T.Z.; methodology, L.F., Y.Z. and L.S.; software, L.F., M.X. and T.Z.; validation, J.L., B.L. and T.Z.; formal analysis, L.F. and Y.Z.; investigation, L.F. and L.S.; resources, L.F., B.L. and T.Z.; data curation, L.F., M.X., J.L. and B.L.; writing—original draft preparation, L.F.; writing—review and editing, T.Z. and Y.Y.; visualization, L.F. and T.Z.; supervision, Y.Z. and L.S.; project administration, Y.Z. and L.S.; funding acquisition, B.L. and Y.Y. All authors have read and agreed to the published version of the manuscript.

Funding: This research was funded by the Electric Power Research Institute of Guizhou Power Grid Co., Ltd., China (contract no. 0666002022030103HX00003).

Institutional Review Board Statement: Not applicable.

Informed Consent Statement: Not applicable.

Data Availability Statement: The raw/processed data required to reproduce these findings cannot be shared at this time for legal or ethical reasons.

Conflicts of Interest: The authors declare no conflict of interest.

References

1. Shu, L.C.; Wang, S.J.; Jiang, X.L.; Hu, Q.; Yang, X.Y.; Yang, S.; Chen, J. Effect of Grading Ring on Ice Characteristics and Flashover Performance of 220 kV Composite Insulators with Different Shed Configurations. *IEEE Trns. Dielectr. Electr. Insul.* **2015**, *22*, 951–960. [[CrossRef](#)]
2. Olad, A.; Maryami, F.; Mirmohseni, A.; Shayegani-Akmal, A.A. Potential of slippery liquid infused porous surface coatings as flashover inhibitors on porcelain insulators in icing, contaminated, and harsh environments. *Prog. Org. Coat.* **2021**, *151*, 106082. [[CrossRef](#)]
3. Li, B.; Bai, J.; He, J.H.; Ding, C.; Dai, X.; Ci, W.J.; Zhu, T.; Liao, R.J.; Yuan, Y. A Review on Superhydrophobic Surface with Anti-Icing Properties in Overhead Transmission Lines. *Coatings* **2023**, *13*, 301. [[CrossRef](#)]
4. Jiang, X.L.; Xiang, Z.; Zhang, Z.J.; Hu, J.L.; Hu, Q.; Shu, L.C. Comparison on ac icing flashover performance of porcelain, glass, and composite insulators. *Cold Reg. Sci. Tech.* **2014**, *100*, 1–7. [[CrossRef](#)]
5. Arianpour, F.; Farzaneh, M.; Kulinich, S.A. Hydrophobic and ice-retarding properties of doped silicone rubber coatings. *Appl. Surf. Sci.* **2013**, *265*, 546–552. [[CrossRef](#)]
6. Jiang, X.L.; Wang, S.H.; Zhang, Z.J.; Xie, S.J.; Wang, Y. Study on AC flashover performance and discharge process of polluted and iced IEC standard suspension insulator string. *IEEE Trans. Power Deliv.* **2007**, *22*, 472–480. [[CrossRef](#)]
7. Sarma, J.; Zhang, L.; Guo, Z.Q.; Dai, X.M. Sustainable icephobicity on durable quasi-liquid surface. *Chem. Eng. J.* **2022**, *431*, 133475. [[CrossRef](#)]
8. Yuan, Y.; Xiang, H.Y.; Liu, G.Y.; Liao, R.J. Fabrication of phase change microcapsules and their applications to anti-icing coating. *Surf. Interfaces* **2021**, *27*, 101516. [[CrossRef](#)]
9. Jiang, X.L.; Fan, C.J.; Xie, Y.B. New method of preventing ice disaster in power grid using expanded conductors in heavy icing area. *IET Gener. Transm. Distrib.* **2019**, *13*, 536–542. [[CrossRef](#)]
10. Zhou, F.; Zhu, J.; An, N.; Wang, C.G.; Liu, J.; Long, L. The anti-icing and deicing robot system for electricity transmission line based on external excitation resonant. *IEEJ Trans. Electr. Electron. Eng.* **2020**, *15*, 593–600. [[CrossRef](#)]
11. Jiang, X.L.; Fan, S.H.; Zhang, Z.J.; Sun, C.X.; Shu, L.C. Simulation and Experimental Investigation of DC Ice-Melting Process on an Iced Conductor. *IEEE Trans. Power Deliv.* **2010**, *25*, 919–929. [[CrossRef](#)]
12. Huang, W.; Huang, J.X.; Guo, Z.G.; Liu, W.M. Icephobic/anti-icing properties of superhydrophobic surfaces. *Adv. Colloid Interface Sci.* **2022**, *304*, 102658. [[CrossRef](#)]

13. Lv, J.Y.; Song, Y.L.; Jiang, L.; Wang, J.J. Bio-Inspired Strategies for Anti-Icing. *ACS Nano* **2014**, *8*, 3152–3169. [[CrossRef](#)]
14. Fan, L.; Li, B.; Wang, Y.; He, J.H.; Bai, J.; Zhu, T.; Yuan, Y. Superhydrophobic Epoxy/Fluorosilicone/PTFE Coatings Prepared by One-Step Spraying for Enhanced Anti-Icing Performance. *Coatings* **2023**, *13*, 569. [[CrossRef](#)]
15. Pan, R.; Zhang, H.J.; Zhong, M.L. Triple-Scale Superhydrophobic Surface with Excellent Anti-Icing and Icephobic Performance via Ultrafast Laser Hybrid Fabrication. *ACS Appl. Mater. Interfaces* **2021**, *13*, 1743–1753. [[CrossRef](#)] [[PubMed](#)]
16. Guo, P.; Zheng, Y.M.; Wen, M.X.; Song, C.; Lin, Y.C.; Jiang, L. Icephobic/Anti-Icing Properties of Micro/Nanostructured Surfaces. *Adv. Mater.* **2012**, *24*, 2642–2648. [[CrossRef](#)] [[PubMed](#)]
17. Feng, L.B.; Yan, Z.N.; Shi, X.T.; Sultonzoda, F. Anti-icing/frosting and self-cleaning performance of superhydrophobic aluminum alloys. *Appl. Phys. A-Mater. Sci. Process.* **2018**, *124*, 142. [[CrossRef](#)]
18. Guo, H.; Xing, Y.; Yuan, H.; Zhang, R.L.; Zhang, Y.F.; Deng, P.Y. Improving the anti-icing performance of superhydrophobic surfaces by nucleation inhibitor. *Surf. Eng.* **2020**, *36*, 621–627. [[CrossRef](#)]
19. Xue, Y.Q.; Wang, Y.B.; Sui, X.; Liang, W.Y.; Wang, F.X. Superhydrophobic, photothermal, MXene/PEI composite film with anti-icing and deicing properties. *Mater. Lett.* **2023**, *347*, 134638. [[CrossRef](#)]
20. Zhang, W.Y.; Gao, N.J.; Li, J.W.; Wu, H.; Izuchukwu, N.K.; Ahmed, S.; Han, E.H.; Liu, F.C. Enhanced anti-icing and anticorrosion properties of nano-SiO₂ composite superhydrophobic coating constructed by a large-scale micropillar array approach. *Prog. Org. Coat.* **2023**, *175*, 107324. [[CrossRef](#)]
21. Liu, Y.; Zhao, Z.B.; Shao, Y.W.; Wang, Y.Q.; Liu, B. Preparation of a superhydrophobic coating based on polysiloxane modified SiO₂ and study on its anti-icing performance. *Surf. Coat. Technol.* **2022**, *437*, 128359. [[CrossRef](#)]
22. Chang, X.T.; Li, M.Y.; Tang, S.K.; Shi, L.; Chen, X.Q.; Niu, S.C.; Zhu, X.J.; Wang, D.S.; Sun, S.B. Superhydrophobic micro-nano structured PTFE/WO₃ coating on low-temperature steel with outstanding anti-pollution, anti-icing, and anti-fouling performance. *Surf. Coat. Technol.* **2022**, *434*, 128214. [[CrossRef](#)]
23. Pan, L.; Xue, P.B.; Wang, M.L.; Wang, F.; Guo, H.X.; Yuan, X.S.; Zhong, L.; Yu, J. Novel superhydrophobic carbon fiber/epoxy composites with anti-icing properties. *J. Mater. Res.* **2021**, *36*, 1695–1704. [[CrossRef](#)]
24. Lei, S.; Wang, F.J.; Fang, X.Z.; Ou, J.F.; Li, W. Icing behavior of water droplets impinging on cold superhydrophobic surface. *Surf. Coat. Technol.* **2019**, *363*, 362–368. [[CrossRef](#)]
25. Zhang, F.; Qian, H.C.; Wang, L.T.; Wang, Z.; Du, C.W.; Li, X.G.; Zhang, D.W. Superhydrophobic carbon nanotubes/epoxy nanocomposite coating by facile one-step spraying. *Surf. Coat. Technol.* **2018**, *341*, 15–23. [[CrossRef](#)]
26. Pan, S.; Wang, N.; Xiong, D.S.; Deng, Y.L.; Shi, Y. Fabrication of superhydrophobic coating via spraying method and its applications in anti-icing and anti-corrosion. *Appl. Surf. Sci.* **2016**, *389*, 547–553. [[CrossRef](#)]
27. Sun, R.Y.; Zhao, J.; Li, Z.; Qin, N.; Mo, J.L.; Pan, Y.J.; Luo, D.B. Robust superhydrophobic aluminum alloy surfaces with anti-icing ability, thermostability, and mechanical durability. *Prog. Org. Coat.* **2020**, *147*, 105745. [[CrossRef](#)]
28. Gao, B.; Du, X.Y.; Liu, Y.Y.; Song, B.R.; Wei, S.H.; Li, Y.H.; Song, Z.X. Candle soot as a template for fabricating superhydrophobic titanium dioxide film by magnetron sputtering. *Vacuum* **2019**, *159*, 29–36. [[CrossRef](#)]
29. Daneshmand, H.; Sazgar, A.; Araghchi, M. Fabrication of robust and versatile superhydrophobic coating by two-step spray method: An experimental and molecular dynamics simulation study. *Appl. Surf. Sci.* **2021**, *567*, 150825. [[CrossRef](#)]
30. Liao, R.J.; Zuo, Z.P.; Guo, C.; Zhuang, A.Y.; Yuan, Y.; Zhao, X.T.; Zhang, Y.Y. Ice accretion on superhydrophobic insulators under freezing condition. *Cold Reg. Sci. Tech.* **2015**, *112*, 87–94. [[CrossRef](#)]
31. Qin, C.; Mulrone, A.T.; Gupta, M.C. Anti-icing epoxy resin surface modified by spray coating of PTFE Teflon particles for wind turbine blades. *Mater. Today Commun.* **2020**, *22*, 100770. [[CrossRef](#)]
32. Chen, H.Y.; Wang, F.F.; Fan, H.Z.; Hong, R.Y.; Li, W.H. Construction of MOF-based superhydrophobic composite coating with excellent abrasion resistance and durability for self-cleaning, corrosion resistance, anti-icing, and loading-increasing research. *Chem. Eng. J.* **2021**, *408*, 127343. [[CrossRef](#)]
33. Farzaneh, M.; Baker, T.; Bernstorff, A.; Brown, K.; Chisholm, W.A.; de Turreil, C.; Drapeau, J.F.; Fikke, S.; George, J.M.; Gnanndt, E.; et al. Insulator icing test methods and procedures a position paper prepared by the IEEE task force on insulator icing test methods. *IEEE Trans. Power Deliv.* **2003**, *18*, 1503–1515. [[CrossRef](#)]
34. Parent, O.; Ilinca, A. Anti-icing and de-icing techniques for wind turbines: Critical review. *Cold Reg. Sci. Tech.* **2011**, *65*, 88–96. [[CrossRef](#)]
35. Zhou, C.; Yin, J.Q. Glaze icing process of moveable overhead conductor and its aerodynamic characteristics with numerical method. *Int. J. Heat Mass Transfer* **2021**, *176*, 121436. [[CrossRef](#)]
36. Hussain, M.M.; Majeed, M.K.; Ma, H.T.; Wang, Y.P.; Saleem, A.; Lotfi, M. PTFE/EP Reinforced MOF/SiO₂ Composite as a Superior Mechanically Robust Superhydrophobic Agent towards Corrosion Protection, Self-Cleaning and Anti-Icing. *Chem.-Eur. J.* **2022**, *28*, e202103220. [[CrossRef](#)]
37. Li, J.; Jiao, W.C.; Wang, Y.C.; Yin, Y.X.; He, X.D. Spraying pressure-tuning for the fabrication of the tunable adhesion superhydrophobic coatings between Lotus effect and Petal effect and their anti-icing performance. *Chem. Eng. J.* **2022**, *434*, 134710. [[CrossRef](#)]
38. Patil, D.; Aravindan, S.; Sarathi, R.; Rao, P.V. Fabrication of self-cleaning superhydrophobic silicone rubber insulator through laser texturing. *Surf. Eng.* **2021**, *37*, 308–317. [[CrossRef](#)]
39. Wang, Y.; Zhao, W.N.; Han, L.; Tam, K.C. Superhydrophobic surfaces from sustainable colloidal systems. *Curr. Opin. Colloid Interface Sci.* **2022**, *57*, 101534. [[CrossRef](#)]

40. Jung, S.; Dorrestijn, M.; Raps, D.; Das, A.; Megaridis, C.M.; Poulikakos, D. Are Superhydrophobic Surfaces Best for Icephobicity? *Langmuir* **2011**, *27*, 3059–3066. [[CrossRef](#)]
41. Ma, Z.C.; Zhao, S.T.; Du, H.R.; Liu, J.Z.; Zhao, H.W.; Ren, L.Q. Simultaneous realization of superhydrophobicity and multiple droplet bouncing through laser ablation, organic adsorption and fluorination treatment. *Mater. Today Phys.* **2022**, *26*, 100739. [[CrossRef](#)]
42. Chu, Z.M.; Jiao, W.C.; Huang, Y.F.; Yan, M.L.; Zheng, Y.T.; Wang, R.G.; He, X.D. Smart Superhydrophobic Films with Self-Sensing and Anti-Icing Properties Based on Silica Nanoparticles and Graphene. *Adv. Mater. Interfaces* **2020**, *7*, 2000492. [[CrossRef](#)]
43. Nepomnyashchy, A.A.; Golovin, A.A.; Tikhomirova, A.E.; Volpert, V.A. Nucleation and growth of droplets at a liquid-gas interface. *Phys. Rev. E* **2006**, *74*, 021605. [[CrossRef](#)]
44. Li, X.L.; Wang, G.Y.; Moita, A.S.; Zhang, C.C.; Wang, S.H.; Liu, Y. Fabrication of bio-inspired non-fluorinated superhydrophobic surfaces with anti-icing property and its wettability transformation analysis. *Appl. Surf. Sci.* **2020**, *505*, 144386. [[CrossRef](#)]
45. Jiang, G.; Chen, L.; Zhang, S.D.; Huang, H.X. Superhydrophobic SiC/CNTs Coatings with Photothermal Deicing and Passive Anti-Icing Properties. *ACS Appl. Mater. Interfaces* **2018**, *10*, 36505–36511. [[CrossRef](#)] [[PubMed](#)]
46. Royaux, A.; El Haitami, A.; Fichet, O.; Cantin, S. Surface free-energy determination of copper wire using a large range of model liquids. *SN Appl. Sci.* **2020**, *2*, 48. [[CrossRef](#)]
47. Bara, M.; Niedźwiedź, M.; Skoneczny, W. Influence of Anodizing Parameters on Surface Morphology and Surface-Free Energy of Al₂O₃ Layers Produced on EN AW-5251 Alloy. *Materials* **2019**, *12*, 695. [[CrossRef](#)]
48. Wang, X.D.; Zhao, H.Y.; Cao, Y.Y.; Su, Y.X.; Hui, H.H.; Shen, J. Surface free energy and microstructure dependent environmental stability of sol-gel SiO₂ antireflective coatings: Effect of combined vapor phase surface treatment. *J. Colloid Interface Sci.* **2019**, *555*, 124–131. [[CrossRef](#)]
49. Jian, Y.M.; Gao, H.T.; Yan, Y.Y. Fabrication of a superhydrophobic micron-nanoscale hierarchical structured surface for delayed icing and reduced frosting. *Surf. Interfaces* **2022**, *34*, 102353. [[CrossRef](#)]
50. Golovin, K.; Kobaku, S.P.R.; Lee, D.H.; DiLoreto, E.T.; Mabry, J.M.; Tuteja, A. Designing durable icephobic surfaces. *Sci. Adv.* **2016**, *2*, e150149. [[CrossRef](#)]
51. Kulinich, S.A.; Farhadi, S.; Nose, K.; Du, X.W. Superhydrophobic Surfaces: Are They Really Ice-Repellent? *Langmuir* **2011**, *27*, 25–29. [[CrossRef](#)] [[PubMed](#)]
52. Zheng, H.K.; Chang, S.N.; Ma, G.J.; Wang, S.S. Anti-icing performance of superhydrophobic surface fabricated by femtosecond laser composited dual-layers coating. *Energy Build.* **2020**, *223*, 110175. [[CrossRef](#)]
53. Boinovich, L.B.; Emelyanenko, K.A.; Emelyanenko, A.M. Superhydrophobic versus SLIPS: Temperature dependence and the stability of ice adhesion strength. *J. Colloid Interface Sci.* **2022**, *606*, 556–566. [[CrossRef](#)] [[PubMed](#)]
54. Szymczyk, K.; Zdziennicka, A.; Jańczuk, B. Adsorption and wetting properties of cationic, anionic and nonionic surfactants in the glass-aqueous solution of surfactant-air system. *Mater. Chem. Phys.* **2015**, *162*, 166–176. [[CrossRef](#)]
55. Kim, H.B.; Lee, W.J.; Choi, S.C.; Lee, K.B.; Lee, M.H. Preparation of PTFE-glass composite filter with low surface free energy by sandblasting. *Surf. Interfaces* **2021**, *26*, 101381. [[CrossRef](#)]
56. Liu, Y.T.; Zhu, D.; Sun, J.W.; Li, J.; Wu, Y.M.; Gao, C.H. Synthesis and characterization of a novel fluorosilicone resin based on trifluoropropylalkoxysilane. *Mater. Chem. Phys.* **2019**, *224*, 40–46. [[CrossRef](#)]
57. Wang, D.H.; Sun, Q.Q.; Hokkanen, M.J.; Zhang, C.L.; Lin, F.Y.; Liu, Q.; Zhu, S.P.; Zhou, T.F.; Chang, Q.; He, B.; et al. Design of robust superhydrophobic surfaces. *Nature* **2020**, *582*, 55–59. [[CrossRef](#)]
58. Wang, N.; Tang, L.L.; Tong, W.; Xiong, D.S. Fabrication of robust and scalable superhydrophobic surfaces and investigation of their anti-icing properties. *Mater. Des.* **2018**, *156*, 320–328. [[CrossRef](#)]
59. Liu, Y.; Shao, Y.W.; Wang, Y.Q.; Wang, J.Y. An abrasion-resistant, photothermal, superhydrophobic anti-icing coating prepared by polysiloxane-modified carbon nanotubes and fluorine-silicone resin. *Colloids Surf. A* **2022**, *648*, 129335. [[CrossRef](#)]

Disclaimer/Publisher’s Note: The statements, opinions and data contained in all publications are solely those of the individual author(s) and contributor(s) and not of MDPI and/or the editor(s). MDPI and/or the editor(s) disclaim responsibility for any injury to people or property resulting from any ideas, methods, instructions or products referred to in the content.